International Journal of Aerospace and Lightweight Structures (IJALS)

TOPOLOGICAL SENSITIVITY ANALYSIS OF STRUCTURAL SOUND RADIATION IN THERMAL ENVIRONMENT*

Xiongwei Yang, Gang Chen and Yueming Li
State Key Laboratory for Strength and Vibration of Mechanical Structures

Xi'an Jiaotong University, Xi'an, 710049, China

Corresponding author:liyueming@mail.xjtu.edu.cn

Received Day Month Year
Revised Day Month Year

Sensitivity analysis is carried out in this paper to minimize the structural sound radiation in thermal environments. The structure studied is subjected to a uniform temperature rise and excited by a time-harmonic surface loading. The compressive thermal stress can reduce the stiffness of the structure, thus changing its radiation property and optimal design. The thermal stress is first evaluated and considered in the following analysis as pre-stress. The dynamic response is calculated through a linear stress-stiffening finite element equation, and the radiated sound power compliance further using Rayleigh integral. The uniform temperature is chosen to be lower than the critical buckling temperature to ensure a linear condition, which needs to be monitored and guaranteed at every iteration during the optimization. Thereafter, the sensitivity analysis is carried out. The particularity of the problem is that if the design variable of one element changes, the thermal stress field of the whole structure will vary; thus the stress stiffness of each element will be different. This will significantly increase the difficulty of the sensitivity analysis and the numerical implementation. The equivalent thermal force which is known as design-dependent load should also be carefully dealt with. Both direct and adjoint methods are discussed, and the latter one is implemented to keep the computational cost at a relatively low level. A bi-material rectangular plate is studied and several numerical cases are discussed.

Keywords: Topology optimization; acoustic power; thermal environment.

1. Introduction

The high thermal and acoustic environments to which the hypersonic vehicles are subjected to during a significant portion of the flight envelop, pose severe challenges to the designers. Compressive thermal stresses due to aerodynamic heating could cause structural buckling and alter the dynamic characteristics. High-intensity acoustic load could cause fatigue of the structure and may paralyze the payload.

Christensen and Sorokin et al [1998] reviewed developments in the structural-acoustic analysis and optimization, and typical objective functions and optimization formulations were discussed. The objective functions although maybe different, measures a level of energy transfer to infinity. Kim and Dong et al [2003] employed sequential FEM and BEM to carry out design sensitivity analysis for structural–acoustic problems. The

* National Natural Science Foundation of China (91016008, 11021202,10902082)

structural dynamic behavior was first obtained through frequency-response analysis, and BEM was used to solve for the pressure response of the acoustic domain. Luo and Gea [2003] employed an approach based on topology optimization to study the optimal configuration of stiffeners for the interior sound reduction in a coupled structural-acoustic system. Yoon and Jensen et al [2007] carried out a structural-acoustic optimization using a mixed finite element formulation, in which displacements as well as pressure are the primal variables. Du and Olhoff [2007, 2010] dealt with the topology optimization problems to minimize the sound power or sum of the pressure square radiated from the structural surface(s) into a surrounding acoustic medium. Akl and El-Sabbagh et al [2009] developed a mathematical model based on FEM to optimize a plate coupled with an acoustic cavity to reduce the fluid-structure interactions at different structural frequencies, verified through experiment by monitoring the vibration and sound radiation into a rigid acoustic cavity of the optimized plates.

Dynamic sensitivity analysis involving thermal stress has also been investigated. It is known that thermal stress may change the stiffness of structure, thus altering its dynamic characteristic [Zienkiewicz and Taylor, 2005]. The particularity of this kind of problems is that if the design variable of one element changes, the thermal stress field of the whole structure will vary. Manickarajah etal [1998] tried to find the optimum thickness distribution of isotropic plate structures to maximize the thermal buckling load using evolutionary method. Although the particularity of the thermal stress was mentioned, the change of the thermal stress on each design variable was neglected by assuming a sufficiently small modification. Pedersen [2001, 2002] optimized the static compliance or eigenvalues of pre-stressed isotropic and laminated plates in MEMS design. The stresses were given at different values to study its influence on the topology. In fact, these thermal stresses are constantly changing in the procedure of the optimization. Chen et al [2003] carried out the analysis of heat conduction, structural stress and buckling are at the same time in the design optimization procedure. However, due to the complexity of the numerical implementation, direct method was used and only several design variables could be considered. Lindgaard and Lund [2010] presented an approach to nonlinear buckling fiber angle optimization of laminated composite shell structures. The derivatives of the geomtetric stiffness (induced by the compressive) were calculated using central difference approximations, which in fact also neglected this particularity. Yang and Li [2012] carried out structural dynamic optimization in thermal environments and fully considered the relationship between the design variablesand the thermal stresses. Adjoint method was employed and very efficient in dealing with large-scaled problems, although quite complex in implementation.

This work can be regarded as an extended work of Yang and Chen etal [2012], in which although the optimization on structural-acoustic in thermal environments was investigated, the relationship between the design variables and the thermal stresses was not fully considered. The sensitivity was localized at element level, indicating that the design variable only affected the thermal stress of the same element.

The thermal stress is first evaluated and used to form the geometric stiffness matrix. Then the structural response in the thermal environment is obtained through the stress stiffening dynamic formula and the acoustic power can be acquired by Rayleigh integral.

Both direct and adjoint methods are discussed to carry out the sensitivity analysis. In direct method, the computational cost can be very high when a large-scale problem is investigated, due to the fact that the geometric stiffness matrix of each element is related to all the design variables. To carry out the simulation more effectively, the adjoint method is implemented.

A bi-material plate subjected to a harmonic force with prescribed amplitude and frequency in a uniform thermal environment is studied. The critical buckling temperature is evaluated to determine the upper limit of the temperature rise, so that a pre-buckling small-deformation can be assumed to establish the dynamic formula in a stress stiffening form [Cook, 1994]. The RAMP interpolation model [Stolpe and Svanberg, 2001] and GCMMA algorithm [Svanberg, 1995] are used in this paper.

2. Dynamic Structure in Thermal Environment

2.1. *Buckling analysis*

When a plate is subjected to temperature rise from the ambient, thermal stress develops in the plate. The thermal stress may induce buckling of the structure when the temperature change is high enough. The optimization is carried out when the plate is in pre-buckling state; thus, the critical buckling temperature T_{cr} is first evaluated to determine the upper limit of the uniform temperature rise. An eigenvalue buckling analysis can be stated as [Cook,1994]

$$\left(\mathbf{K}+\lambda\mathbf{K}_{\mathrm{G}}\right)\mathbf{\Phi}=\mathbf{0} \tag{2.1}$$

where λ is a scalar multiplier, $\mathbf{\Phi}$ is the eigenvector and $\mathbf{K}$ is the stiffness matrix. $\Delta T=T_1-T_0$ is the temperature change. With the initial temperature $T_0=0\,^{\circ}\mathrm{C}$, the product of λ and the thermal load ΔT yields T_{cr}.

$\mathbf{K}_{\mathrm{G}}$ refers to the geometric stiffness for bending induced by the in-plane thermal stress [Zienkiewicz and Taylor, 2005]

$$\mathbf{K}_{\mathrm{G}}=\sum_{l}\int_{A_l}\mathbf{G}^{\mathrm{T}}\mathbf{S}\mathbf{G}dA \tag{2.2}$$

where $\mathbf{S}$ is the membrane stress matrix at the element level; $\mathbf{G}$ is a non-linear strain-displacement matrix; A_l is area of element l.

2.2. *Membrane stress*

If the temperature change across the thickness is uniform, the thermo-elastic problem of the plate can be described with the plane-stress constitutive equation,

$$\boldsymbol{\sigma}=\mathbf{D}_{\mathrm{m}}\left(\boldsymbol{\varepsilon}-\alpha\Delta\mathbf{T}\right)=E\mathbf{D}\boldsymbol{\varepsilon}-\beta\mathbf{D}\Delta\mathbf{T} \tag{2.3}$$

where $\boldsymbol{\sigma}$ is the membrane stress vector, comprised of the same components as the membrane stress matrix $\mathbf{S}$; E, α, $\beta=E\alpha$ are the elastic modulus, the thermal expansion coefficient and the thermal stress coefficient respectively; $\mathbf{D}_{\mathrm{m}}$ is the membrane elasticity matrix; $\Delta\mathbf{T}$ is the temperature rise vector.

The strain in Eq.(2.3) can be written in FE form

$$\boldsymbol{\varepsilon} = \mathbf{B}\mathbf{U}_{tl} \tag{2.4}$$

where $\mathbf{B}$ is a strain-displacement matrix; $\mathbf{U}_{tl}$ is the element displacement vector, which can be obtained with the boundary conditions through

$$\mathbf{K}\mathbf{U}_{\mathrm{t}} = \mathbf{F}_{\mathrm{t}} \tag{2.5}$$

where $\mathbf{F}_{\mathrm{t}}$ is the equivalent thermal force induced by the uniform temperature rise; $\mathbf{U}_{\mathrm{t}}$ is the thermal displacement; the index "t" denotes the word "thermal".
The equivalent membrane thermal force $\mathbf{F}_{\mathrm{t}}$ has the form [Zienkiewicz and Taylor, 2005]

$$\mathbf{F}_{\mathrm{t}} = -\sum_{l}\int_{A_l} \alpha \mathbf{B}^{\mathrm{T}}\mathbf{D}_{\mathrm{m}}\Delta\mathbf{T}dA = -\sum_{l}\int_{A_l} \beta \mathbf{B}^{\mathrm{T}}\mathbf{D}\Delta\mathbf{T}dA \tag{2.6}$$

Eq.(2.6) indicates that the equivalent thermal force is design-dependent. For the bi-material topology optimization problem, both the elastic modulus and the thermal expansion coefficient have to be switched simultaneously from one material to the other. Incompatibility may occur between the stiffness and the thermal load. By introducing the thermal stress coefficient β, the penalty can be made properly to the thermal load $\mathbf{F}_{\mathrm{t}}$, and the incompatibility can be efficiently avoided [Gao and Zhang, 2010].

2.3. *Dynamic formula*

When the temperature is below T_{cr}, the dynamic FE formula of the plate in a uniform thermal environment can be written in a stress stiffening form (with the damping neglected) [Cook, 1994]

$$\left(\mathbf{K} + \mathbf{K}_{\mathrm{G}} - \omega^2\mathbf{M}\right)\mathbf{U} = \mathbf{F} \tag{2.7}$$

where $\mathbf{K}$, $\mathbf{M}$ are the stiffness and mass matrices respectively; $\mathbf{F}$ is the amplitude vector of the time-harmonic external load; $\omega=2\pi f$ is the circle frequency; $\mathbf{U}$ is the dynamic displacement response vector.The surface velocity can be obtained

$$\mathbf{V} = -i\omega\mathbf{U}_{\mathrm{n}} \tag{2.8}$$

$\mathbf{U}_{\mathrm{n}}$ is the normal displacement of the plate, i.e. the transverse displacement component.

3. Finite Element Discretization for Radiated Power

Consider a vibrating plate mounted on a rigid baffle and placed in a light fluid such as air. The pressure p at any observation point $\mathbf{r}$ on the surface of the plate can be described using Rayleigh integral as

$$p = j\rho_0\omega\int_A v_a G\left(\mathbf{r}-\mathbf{r}_a\right)dA \tag{3.1}$$

where v_a refers to the normal surface velocity at point $\mathbf{r}_a$; ρ_0 indicates the density of air; $G(\mathbf{r}\text{-}\mathbf{r}_{\mathrm{a}})$ is the half-space Green's function

$$G\left(\mathbf{r}-\mathbf{r}_a\right)=\frac{e^{-jk|\mathbf{r}-\mathbf{r}_a|}}{2\pi|\mathbf{r}-\mathbf{r}_a|} \tag{3.2}$$

k=ω/c is the wave number and c is the speed of sound in air.
The acoustic power radiated from the vibrating plate can then be written as

$$\begin{aligned} W &= \int_A \frac{1}{2}\mathrm{Re}\left(pv^*\right)\mathrm{d}A \\ &= \frac{j\rho_0\omega}{4\pi}\int_A\int_A v_a\frac{e^{-jk|\mathbf{r}-\mathbf{r}_a|}}{|\mathbf{r}-\mathbf{r}_a|}dAv^*dA \\ &= \frac{\rho_0\omega}{4\pi}\int_A\int_A v_a\frac{\sin k|\mathbf{r}-\mathbf{r}_a|}{|\mathbf{r}-\mathbf{r}_a|}dAv^*dA \end{aligned} \tag{3.3}$$

where * indicates complex conjugation of the quantity.
Note that when $\mathbf{r}$ = $\mathbf{r}_a$, sin(k|$\mathbf{r}$-$\mathbf{r}_a$|)/|$\mathbf{r}$-$\mathbf{r}_a$| approaches k and the singularity can be avoided; the reciprocal property that p($\mathbf{r}$) due to unit velocity at $\mathbf{r}_a$ is equal to p($\mathbf{r}_a$) due to unit velocity at $\mathbf{r}$ is used to simplify Eq.(3.3).
Restate Eq. (3.3) in FE form

$$W=\frac{\rho_0\omega}{4\pi}\sum\sum v_a^{\mathrm{T}}J_a\frac{\sin k|\mathbf{r}-\mathbf{r}_a|}{|\mathbf{r}-\mathbf{r}_a|}Jv^*=\mathbf{V}^*\mathbf{Z}_v\mathbf{V}=\mathbf{U}_{\mathrm{n}}^*\mathbf{Z}\mathbf{U}_{\mathrm{n}} \tag{3.4}$$

Note that single point Gaussian quadrature is used. v_a and v are now the normal velocity at the centroids ($\mathbf{r}_{\mathrm{a}}$ and $\mathbf{r}$) of the element. J_a and J are the values of the Jacobian at the element centers.

4. Optimization Problem and Sensitivity Analysis

4.1. *Problem formulation*

The topology optimization problem for minimizing the radiated sound power of the bi-material plate in the thermal environment can be stated as

$$\begin{aligned} \min\ \ & W=\int_A\frac{1}{2}\mathrm{Re}\left(pv^*\right)\mathrm{d}A \\ s.t.\ \ & \left(\mathbf{K}+\mathbf{K}_{\mathrm{G}}-\omega^2\mathbf{M}\right)\mathbf{U}=\mathbf{F} \\ & \mathbf{K}\mathbf{U}_{\mathrm{t}}=\mathbf{F}_{\mathrm{t}} \\ & p=j\rho_0\omega\int_A v_aG\left(\mathbf{r}-\mathbf{r}_a\right)dA \\ & \sum_l V_l\zeta_l\le V \\ & \zeta_l\in(0,1) \end{aligned} \tag{4.1}$$

where ζ_l is the design variable, denoting the artificial volume fraction of material 1 (the stiffer of the two materials) in the element l; V_l is the volume of the element l; V is the maximum volume of material 1 of the structure.

At each iteration, the second constraint equation is first assembled and solved to calculate the displacement $\mathbf{U}_t$. With Eqs.(2.4) and (2.5), the membrane thermal stress $\boldsymbol{\sigma}$ can be obtained to get the geometric stiffness matrix $\mathbf{K}_G$. The first constraint equation can then be solved to obtain the structural response. The third constraint equation describes the sound radiation from baffled vibrating plate. Note that the feedback is neglected and this is a sequential vibro-acoustic problem.

4.2. *Interpolation model*

The RAMP interpolation models [Stolpe and Svanberg, 2001] of the elastic modulus, the mass density and the thermal stress coefficient can be written as

$$\begin{aligned} E_l &= R(\zeta_l)E^{(1)} + (1-R(\zeta_l))E^{(0)} \\ \rho_l &= R(\zeta_l)\rho^{(1)} + (1-R(\zeta_l))\rho^{(0)} \\ \beta_l &= R(\zeta_l)\beta^{(1)} + (1-R(\zeta_l))\beta^{(0)} \end{aligned} \tag{4.2}$$

where the superscripts 0 and 1 denote material 0 and material 1 respectively;

$$R(\zeta_l) = \frac{\zeta_l}{1+p(1-\zeta_l)} \tag{4.3}$$

and p is the penalty factor.

4.3. *Sensitivity analysis*

The sensitivity of the objective function W can be written as

$$\frac{\mathrm{d}W}{\mathrm{d}\zeta_l} = \frac{\mathrm{d}\mathbf{U}_{\mathrm{n}}^*}{\mathrm{d}\zeta_l}\mathbf{Z}\mathbf{U}_{\mathrm{n}} + \mathbf{U}_{\mathrm{n}}^*\frac{\mathrm{d}\mathbf{Z}}{\mathrm{d}\zeta_l}\mathbf{U}_{\mathrm{n}} + \mathbf{U}_{\mathrm{n}}^*\mathbf{Z}\frac{\mathrm{d}\mathbf{U}_{\mathrm{n}}}{\mathrm{d}\zeta_l} = 2\mathbf{U}_{\mathrm{n}}^*\mathbf{Z}\frac{\mathrm{d}\mathbf{U}_{\mathrm{n}}}{\mathrm{d}\zeta_l} \tag{4.4}$$

The design variable in this work is the artificial volume fraction of material 1, and the structure is subjected to harmonic load with a prescribed frequency; thus the derivative of matrix $\mathbf{Z}$ to ζ_l is zero.

According to Eq.(3.5), the displacement derivative can be obtained by differentiating Eq.(2.7)at element level.

$$(\mathbf{K}+\mathbf{K}_{\mathrm{G}}-\omega^2\mathbf{M})\frac{\mathrm{d}\mathbf{U}}{\mathrm{d}\zeta_l} = -\left(\frac{\mathrm{d}\mathbf{K}}{\mathrm{d}\zeta_l} + \frac{\mathrm{d}\mathbf{K}_{\mathrm{G}}}{\mathrm{d}\zeta_l} - \omega^2\frac{\mathrm{d}\mathbf{M}}{\mathrm{d}\zeta_l}\right)\mathbf{U} \tag{4.5}$$

Note that the surface loading $\mathbf{F}$ is design-independent. It also should be noticed that, if one design variable ζ_l changes, the membrane thermal stress of all the elements will vary, so will all the $\mathbf{K}_G$. Thus, Eq. (4.5) can be written as

$$\left(\mathbf{K}_l+\mathbf{K}_{\mathrm{G}l}-\omega^2\mathbf{M}_l\right)\frac{\mathrm{d}\mathbf{U}_l}{\mathrm{d}\zeta_l}=-\left(\frac{\mathrm{d}\mathbf{K}_l}{\mathrm{d}\zeta_l}-\omega^2\frac{\mathrm{d}\mathbf{M}_l}{\mathrm{d}\zeta_l}\right)\mathbf{U}_l-\sum_m\frac{\mathrm{d}\mathbf{K}_{\mathrm{G}m}}{\mathrm{d}\zeta_l}\mathbf{U}_m \tag{4.6}$$

The derivatives of **K** and **M** in Eq.(4.5) at the element level are as follows,

$$\begin{aligned}\frac{\mathrm{d}\mathbf{K}_l}{\mathrm{d}\zeta_l}&=\frac{1+p}{\left(1+p\left(1-\zeta_l\right)\right)^2}\left(\mathbf{K}_l^{(1)}-\mathbf{K}_l^{(0)}\right)\\ \frac{\mathrm{d}\mathbf{M}_l}{\mathrm{d}\zeta_l}&=\frac{1+p}{\left(1+p\left(1-\zeta_l\right)\right)^2}\left(\mathbf{M}_l^{(1)}-\mathbf{M}_l^{(0)}\right)\end{aligned} \tag{4.7}$$

4.3.1. *Direct method*

In direct method, Eq.(4.5) needs to be solved to get the derivative of the thermal displacement. The key is the derivative of the geometric stiffness matrix $\mathbf{K}_{\mathrm{G}}$; it involves not only the temperature change, but also the strain induced by the equivalent thermal force. With Eq.(2.3), the membrane stress **S** in Eq.(2.2) can be stated as

$$\mathbf{S}=E\boldsymbol{\Xi}-\beta\boldsymbol{\Theta} \tag{4.8}$$

where $E\boldsymbol{\Xi}$, $\beta\boldsymbol{\Theta}$ refer to the strain part and the thermal expansion part respectively. Thus the geometric stiffness matrix can be divided as follows

$$\begin{aligned}\mathbf{K}_{\mathrm{G}}&=\sum_m\int_{A_m}\mathbf{G}^{\mathrm{T}}\mathbf{S}\mathbf{G}dA\\ &=\sum_m\int_{A_m}\mathbf{G}^{\mathrm{T}}\left(E_m\boldsymbol{\Xi}-\beta_m\boldsymbol{\Theta}\right)\mathbf{G}dA\\ &=\sum_m\int_{A_m}E_m\mathbf{G}^{\mathrm{T}}\boldsymbol{\Xi}\mathbf{G}dA-\sum_m\int_{A_m}\beta_m\mathbf{G}^{\mathrm{T}}\boldsymbol{\Theta}\mathbf{G}dA\end{aligned} \tag{4.9}$$

Accordingly the partial derivative of the geometric stiffness matrix for the element *m* can be written as

$$\frac{\mathrm{d}\mathbf{K}_{\mathrm{G}m}}{\mathrm{d}\zeta_l}=\frac{\mathrm{d}E_m}{\mathrm{d}\zeta_l}\int_{A_m}\mathbf{G}^{\mathrm{T}}\boldsymbol{\Xi}\mathbf{G}dA+E_m\int_{A_m}\mathbf{G}^{\mathrm{T}}\frac{\mathrm{d}\boldsymbol{\Xi}}{\mathrm{d}\zeta_l}\mathbf{G}dA-\frac{\mathrm{d}\beta_m}{\mathrm{d}\zeta_l}\int_{A_m}\mathbf{G}^{\mathrm{T}}\boldsymbol{\Theta}\mathbf{G}dA \tag{4.10}$$

It can be found that only the second part of the right-hand items is left to deal with, that is, the derivative of the *m*th element's thermal strain.

Since the membrane stress **S** has been restated as Eq.(4.8) according to Eq.(2.3), the derivative of $\boldsymbol{\Xi}$ is in fact equivalent to the derivative of $\boldsymbol{\varepsilon}$, both referring to the derivatives of the membrane strains. It is as follows with Eq.(2.4)

$$\frac{\mathrm{d}\boldsymbol{\varepsilon}}{\mathrm{d}\zeta_l}=\frac{\mathrm{d}\left(\mathbf{B}\mathbf{U}_{tm}\right)}{\mathrm{d}\zeta_l}=\mathbf{B}\frac{\mathrm{d}\mathbf{U}_{tm}}{\mathrm{d}\zeta_l} \tag{4.11}$$

The derivative of the thermal displacement in Eq. (4.11) can be obtained through differentiating Eq.(2.5)

$$\frac{\mathrm{d}\left(\mathbf{K}\mathbf{U}_{\mathrm{t}}\right)}{\mathrm{d}\zeta_l}=\frac{\mathrm{d}\mathbf{F}_{\mathrm{t}}}{\mathrm{d}\zeta_l} \tag{4.12}$$

$$\mathbf{K}_m\frac{\mathrm{d}\mathbf{U}_{tm}}{\mathrm{d}\zeta_l}=-\frac{\mathrm{d}\mathbf{K}_m}{\mathrm{d}\zeta_l}\mathbf{U}_{\mathrm{t}}+\frac{\mathrm{d}\mathbf{F}_{tm}}{\mathrm{d}\zeta_l} \tag{4.13}$$

Note that $\mathbf{F}_{\mathrm{t}}$ is design-dependent and related to the thermal stress coefficient β; $\mathrm{d}\mathbf{F}_{tm}/\mathrm{d}\zeta_l=0$ if $m\neq l$. According Eq.(2.6), the derivation of $\mathbf{F}_{\mathrm{t}}$ can be written as

$$\frac{\mathrm{d}\mathbf{F}_{tl}}{\mathrm{d}\zeta_l}=\frac{\mathrm{d}\beta_l}{\mathrm{d}\zeta_l}\int_{A_l}\mathbf{B}^{\mathrm{T}}\mathbf{D}\Delta\mathbf{T}dA \tag{4.14}$$

To obtain the derivative of thermal displacement in Eq.(4.11), the global form of Eq.(4.13) should be assembled and then solved with the boundary conditions.

In this direct method, the computer cost can be huge for large-scale problems, since Eq.(4.13) needs to be solved for the sensitivity on each design variable in every iteration.

4.3.2. *Adjoint method*

In order to keep the computational cost at a reasonable level, adjoint method is discussed and implemented. Eq.(4.4) can be written as follows by introducing adjoint factors,

$$\begin{aligned}\frac{\mathrm{d}W}{\mathrm{d}\zeta_l}=&2\mathbf{U}_{\mathrm{n}}^{*}\mathbf{Z}\frac{\mathrm{d}\mathbf{U}_{\mathrm{n}}}{\mathrm{d}\zeta_l}\\&+\boldsymbol{\Lambda}_1^{\mathrm{T}}\left(\left(\mathbf{K}+\mathbf{K}_{\mathrm{G}}-\omega^2\mathbf{M}\right)\frac{\mathrm{d}\mathbf{U}}{\mathrm{d}\zeta_l}+\left(\frac{\mathrm{d}\mathbf{K}}{\mathrm{d}\zeta_l}+\frac{\mathrm{d}\mathbf{K}_{\mathrm{G}}}{\mathrm{d}\zeta_l}-\omega^2\frac{\mathrm{d}\mathbf{M}}{\mathrm{d}\zeta_l}\right)\mathbf{U}\right)\\&+\boldsymbol{\Lambda}_2^{\mathrm{T}}\left(\frac{\mathrm{d}\mathbf{K}}{\mathrm{d}\zeta_l}\mathbf{U}_{\mathrm{t}}+\mathbf{K}\frac{\mathrm{d}\mathbf{U}_{\mathrm{t}}}{\mathrm{d}\zeta_l}-\frac{\mathrm{d}\mathbf{F}_{\mathrm{t}}}{\mathrm{d}\zeta_l}\right)\end{aligned} \tag{4.15}$$

It can be seen from Eq.(4.10) $\mathbf{K}_{\mathrm{G}}$ is the function of $\mathbf{U}_{\mathrm{t}}$, E, β, ζ, so the derivatives of $\mathbf{K}_{\mathrm{G}}$ can be rewritten as,

$$\frac{\mathrm{d}\mathbf{K}_{\mathrm{G}}}{\mathrm{d}\zeta_l}=\left(\frac{\partial\mathbf{K}_{\mathrm{G}}}{\partial\mathbf{U}_{\mathrm{t}}}\right)^{\mathrm{T}}\frac{\partial\mathbf{U}_{\mathrm{t}}}{\partial\zeta_l}+\frac{\partial\mathbf{K}_{\mathrm{G}}}{\partial\mathbf{E}}\frac{\partial\mathbf{E}}{\partial\zeta_l}+\frac{\partial\mathbf{K}_{\mathrm{G}}}{\partial\boldsymbol{\beta}}\frac{\partial\boldsymbol{\beta}}{\partial\zeta_l} \tag{4.16}$$

where $\mathbf{E}$, $\boldsymbol{\beta}$ are the vectors of the elastic modulus and the thermal expansion coefficient respectively. Eq.(4.15) can be rearranged as

$$\begin{aligned}\frac{\mathrm{d}W}{\mathrm{d}\zeta_l}=&2\mathbf{U}_{\mathrm{n}}^{*}\mathbf{Z}\frac{\mathrm{d}\mathbf{U}_{\mathrm{n}}}{\mathrm{d}\zeta_l}+\boldsymbol{\Lambda}_1^{\mathrm{T}}\left(\mathbf{K}+\mathbf{K}_{\mathrm{G}}-\omega^2\mathbf{M}\right)\frac{\mathrm{d}\mathbf{U}}{\mathrm{d}\zeta_l}\\&+\boldsymbol{\Lambda}_1^{\mathrm{T}}\left(\frac{\partial\mathbf{K}_{\mathrm{G}}}{\partial\mathbf{U}_{\mathrm{t}}}\right)^{\mathrm{T}}\frac{\partial\mathbf{U}_{\mathrm{t}}}{\partial\zeta_l}\mathbf{U}+\boldsymbol{\Lambda}_2^{\mathrm{T}}\mathbf{K}\frac{\mathrm{d}\mathbf{U}_{\mathrm{t}}}{\mathrm{d}\zeta_l}\\&+\boldsymbol{\Lambda}_1^{\mathrm{T}}\left(\frac{\mathrm{d}\mathbf{K}}{\mathrm{d}\zeta_l}+\frac{\partial\mathbf{K}_{\mathrm{G}}}{\partial\mathbf{E}}\frac{\partial\mathbf{E}}{\partial\zeta_l}+\frac{\partial\mathbf{K}_{\mathrm{G}}}{\partial\boldsymbol{\beta}}\frac{\partial\boldsymbol{\beta}}{\partial\zeta_l}-\omega^2\frac{\mathrm{d}\mathbf{M}}{\mathrm{d}\zeta_l}\right)\mathbf{U}+\boldsymbol{\Lambda}_2^{\mathrm{T}}\left(\frac{\mathrm{d}\mathbf{K}}{\mathrm{d}\zeta_l}\mathbf{U}_{\mathrm{t}}-\frac{\mathrm{d}\mathbf{F}_{\mathrm{t}}}{\mathrm{d}\zeta_l}\right)\end{aligned} \tag{4.17}$$

To avoid the derivatives of $\mathbf{U}$ and $\mathbf{U}_t$,

$$2\mathbf{U}_n^* \mathbf{Z} \frac{\mathrm{d}\mathbf{U}_n}{\mathrm{d}\zeta_l} + \mathbf{\Lambda}_1^T \left(\mathbf{K} + \mathbf{K}_G - \omega^2 \mathbf{M}\right) \frac{\mathrm{d}\mathbf{U}}{\mathrm{d}\zeta_l} = 0 \tag{4.18}$$

$$\mathbf{\Lambda}_1^T \left(\frac{\partial \mathbf{K}_G}{\partial \mathbf{U}_t}\right)^T \frac{\partial \mathbf{U}_t}{\partial \zeta_l} \mathbf{U} + \mathbf{\Lambda}_2^T \mathbf{K} \frac{\mathrm{d}\mathbf{U}_t}{\mathrm{d}\zeta_l} = 0 \tag{4.19}$$

Please note that since $\partial E_m/\partial\zeta_l$, $\partial\beta_m/\partial\zeta_l$, $\mathrm{d}\mathbf{K}_m/\mathrm{d}\zeta_l$, $\mathrm{d}\mathbf{M}_m/\mathrm{d}\zeta_l$, $\mathrm{d}\mathbf{F}_{tm}/\mathrm{d}\zeta_l$ equal 0 when $m \neq l$, Eq.(4.17) can be written as

$$\begin{aligned} \frac{\mathrm{d}W}{\mathrm{d}\zeta_l} = {} & \mathbf{\Lambda}_{1l}^T \left(\frac{\mathrm{d}\mathbf{K}_l}{\mathrm{d}\zeta_l} + \frac{\partial \mathbf{K}_G}{\partial E_l} \frac{\partial E_l}{\partial \zeta_l} + \frac{\partial \mathbf{K}_G}{\partial \beta}_l \frac{\partial \beta_l}{\partial \zeta_l} - \omega^2 \frac{\mathrm{d}\mathbf{M}_l}{\mathrm{d}\zeta_l} \right) \mathbf{U}_l \\ & + \mathbf{\Lambda}_{2l}^T \left(\frac{\mathrm{d}\mathbf{K}_l}{\mathrm{d}\zeta_l} \mathbf{U}_{tl} - \frac{\mathrm{d}\mathbf{F}_{tl}}{\mathrm{d}\zeta_l} \right) \end{aligned} \tag{4.20}$$

where $\mathbf{\Lambda}_1$, $\mathbf{\Lambda}_2$ are the solutions of the Eqs.(4.18) and (4.19). Considering the relationship between $\mathrm{d}\mathbf{U}_n/\mathrm{d}\zeta_l$ and $\mathrm{d}\mathbf{U}/\mathrm{d}\zeta_l$

$$\frac{\mathrm{d}\mathbf{U}_n}{\mathrm{d}\zeta_l} = \mathbf{L} \frac{\mathrm{d}\mathbf{U}}{\mathrm{d}\zeta_l} \tag{4.21}$$

Eq.(4.18) can be written as

$$\left(\mathbf{K} + \mathbf{K}_G - \omega^2 \mathbf{M}\right) \mathbf{\Lambda}_1 = -2\left(\mathbf{U}_n^* \mathbf{Z} \mathbf{L}\right)^T \tag{4.22}$$

where $\mathbf{L}$ is a transformation matrix which can be easily obtained.
Eq.(4.19) can be stated at element level,

$$\mathbf{\Lambda}_{1m}^T \left(\frac{\partial \mathbf{K}_{Gm}}{\partial \mathbf{U}_{tm}}\right)^T \frac{\partial \mathbf{U}_{tm}}{\partial \zeta_l} \mathbf{U}_m + \mathbf{\Lambda}_{2m}^T \mathbf{K}_m \frac{\mathrm{d}\mathbf{U}_{tm}}{\mathrm{d}\zeta_l} = 0 \tag{4.23}$$

Note that

$$\left(\frac{\partial \mathbf{K}_{Gm}}{\partial \mathbf{U}_{tm}}\right)^T \frac{\partial \mathbf{U}_{tm}}{\partial \zeta_l} = \left(\frac{\partial \mathbf{K}_{Gm}}{\partial U_{tm1}}\right)^T \frac{\partial U_{tm1}}{\partial \zeta_l} + \left(\frac{\partial \mathbf{K}_{Gm}}{\partial U_{tm2}}\right)^T \frac{\partial U_{tm2}}{\partial \zeta_l} + \ldots + \left(\frac{\partial \mathbf{K}_{Gm}}{\partial U_{tmn}}\right)^T \frac{\partial U_{tmn}}{\partial \zeta_l} \tag{4.24}$$

where n is the total number of the element DOFs and U_{tmn} is the displacement at the nth DOF of the mth element. Thus, the first item in Eq.(4.23) at nth DOF can be written as

$$\mathbf{\Lambda}_{1m}^T \left(\frac{\partial \mathbf{K}_{Gm}}{\partial U_{tmn}}\right)^T \mathbf{U}_m \frac{\partial U_{tmn}}{\partial \zeta_l} \tag{4.25}$$

Note that the product of the first three items is scalar, and the relationship between $\mathbf{K}_{Gm}$ and U_{tmn} is linear [Cook, 1994],

$$\frac{\partial \mathbf{K}_{Gm}}{\partial U_{tmn}} = \frac{\mathbf{K}_{Gm}\left(U_{tmn} + \Delta u_{mn}\right)}{\Delta u_{mn}} \tag{4.26}$$

where Δu_{mn} is the displacement change at the nth DOF of the mth element.
Eq.(4.23) can be written as

$$\mathbf{\Lambda}_{1m}^{\mathrm{T}}\left(\frac{\partial \mathbf{K}_{Gm}}{\partial \mathbf{U}_{tm}}\right)^{\mathrm{T}} \mathbf{U}_m \frac{\partial \mathbf{U}_{tm}}{\partial \zeta_l} + \mathbf{\Lambda}_{2m}^{\mathrm{T}} \mathbf{K}_m \frac{\mathrm{d}\mathbf{U}_{tm}}{\mathrm{d}\zeta_l} = 0 \tag{4.27}$$

that is,

$$\mathbf{K}_m \mathbf{\Lambda}_{2m} = -\mathbf{U}_m^{\mathrm{T}} \frac{\partial \mathbf{K}_{Gm}}{\partial \mathbf{U}_{tm}} \mathbf{\Lambda}_{1m} \tag{4.28}$$

With Eqs(4.22) and (4.28), $\mathbf{\Lambda}_1$, $\mathbf{\Lambda}_2$ can be obtained. Since only these two equations need to be solved in the sensitivity analysis at each iteration, the computational cost is effectively controlled.

5. Numerical Examples

A four-edge clamped bi-material square plate with dimension 1m×1m×0.02m is studied. The plate is subjected to a temperature rise $\Delta T = T_1 - T_0$ with $T_0 = 0\,^{o}\mathrm{C}$. The specific mass of the fluid (i.e. air) is $\rho_0 = 1.21\mathrm{kg/m}^3$ and the sound speed c = 343.4m/s. The material properties are as follows:
$E^{(0)}$ = 70GPa, $\rho^{(0)} = 2650\mathrm{kg/m}^3$, $\alpha^{(0)} = 1.5\times10^{-5}\,^{o}\mathrm{C}^{-1}$
$E^{(1)}$ = 210GPa, $\rho^{(1)} = 6500\mathrm{kg/m}^3$, $\alpha^{(1)} = 1.1\times10^{-5}\,^{o}\mathrm{C}^{-1}$
A mesh of 40×40 with isoparametric 4-node element is used here and there are 1600 design variables. The artificial control volume fraction of material 1 is 50%, uniformly distributed for the initial structure. A harmonic surface load with 1N amplitude is applied at all the nodes of the mesh.
GCMMA [Svanberg, 1995], the globally convergent version of MMA [Svanberg, 1987] is employed.
Filtering of the sensitivity is implemented to control the checkerboards [Bendsøe and Sigmund, 2003]. The filtering radius is 1.5x dimension of the element.
p =3 *is* used in the following calculations.

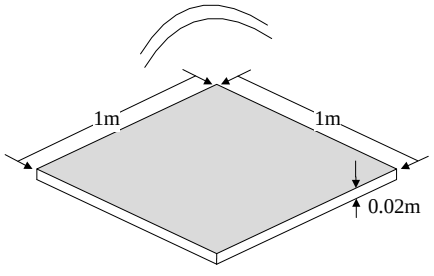

Fig.1 Acoustic radiation from the four-edge clamped square plate

5.1. *Eigenvalue and buckling analysis*

T_{cr} = 100.8 °C is first evaluated by carrying out an eigenvalue buckling analysis Eq.(2.1). It serves as the upper limit of ΔT, to ensure that the uniform temperature rise does not induce buckling of the initial plate.

Four thermal cases, i.e. ΔT = 0 °C, ΔT = 50 °C, ΔT = 75 °C, ΔT = 90 °C, are chosen in this work. It is shown later from the numerical results that T_{cr} basically increases as the optimization proceeds, indicating that the plate is always in the pre-buckling state.

The first 15 order frequencies of the initial plate are obtained, shown in Fig.1. It can be found that the natural frequencies decrease as the temperature rises. The fundamental frequencies are 184.2Hz, 131.8Hz, 94.4Hz and 61.3Hz respectively.

According to the eigenvalue analysis, three excitation frequency cases are selected, that is, *f*=50Hz, 250Hz, 1000Hz. *f*=50Hz is below all the fundamental frequencies of the initial plate in the four thermal environments; *f*=250Hz is higher than the fundamental frequencies but lower than the 2nd order frequencies; case *f*=1000Hz is a relatively high-frequency case.

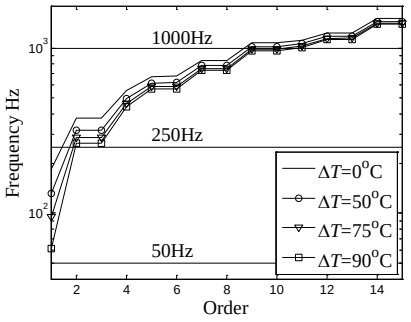

Fig.1 First 15 natural frequencies and 3 excitation frequencies

5.2. *Results and discussions*

5.2.1. *Case f=50Hz*

The optimal topology and the iteration history of the sound power level (SPL) are shown in Figs.2 and 3 respectively.

It can be seen that the topology of the structure remains similar in different thermal environments, except that the central part becomes a little smaller. The SPL is 83.9dB, 90.0dB, 97.0dB, 111.0 dB initially and decreases 67.8%, 81.9%, 93.4% and 99.5% respectively after optimization. With increase of the temperature change, the natural frequencies decrease and the structure tends to resonate; thus the SPL becomes higher. As the iteration goes on, the fundamental frequency rises (Fig.4), and the gap between the fundamental and the excitation frequencies becomes larger; therefore the SPL decreases.

Fig.2 Topology of the bi-material plate (white: material 0; black: material 1) of the case f=50Hz in the four thermal environments a ΔT = 0 °C, b ΔT = 50 °C, c ΔT = 75 °C, d ΔT = 90 °C (from left)

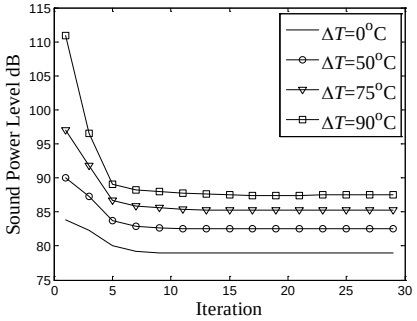

Fig.3 iteration history of the sound power level of the case f=50Hz

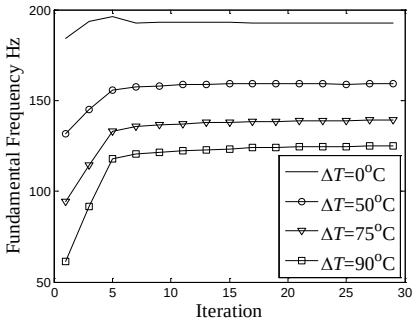

Fig.4 iteration history of the sound power level of the case f=50Hz

It can be found in Fig.5 that during the optimization, T_{cr} increases with the iteration, indicating the structure is always in the pre-buckling state.

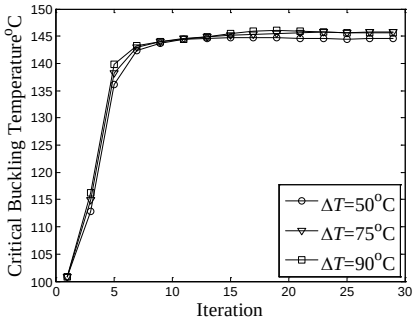

Fig.5 Iteration history of the critical buckling temperature of the case *f*=50Hz

5.2.2. *Case f=250Hz*

The optimal topology and the iteration history of the SPL are shown in Figs.6 and 7 respectively.

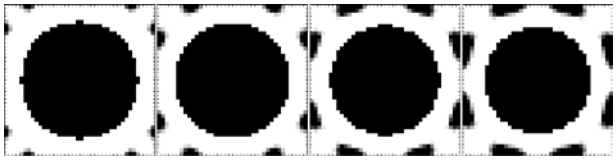

Fig.6 Topology of the bi-material plate (white: material 0; black: material 1) of the case *f*=250Hz in the four thermal environments a ΔT = 0 °C, b ΔT = 50 °C, c ΔT = 75 °C, d ΔT = 90 °C (from left)

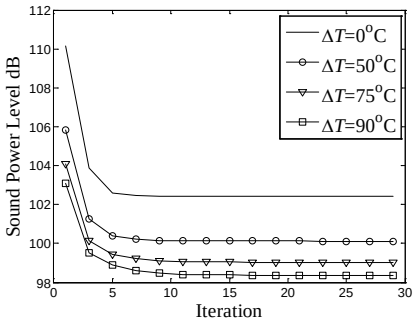

Fig.7 iteration history of the sound power level of the case *f*=50Hz

Like the case *f*=50Hz, the basic topology remains similar in different thermal environments. The initial SPL of the four subcases are 110.2 dB, 105.8 dB, 104.1dB, 103.1dB, and decreases 83.2%, 73.2%, 68.7%, 66.2% respectively after optimization.

The increase of SPL with temperature implies that the fundamental frequency is probably the main component that affects the response. If this is not the case, then the second natural frequency one will be the main component. Due to the fact that the natural frequencies decrease with the temperature, SPL verse the temperature may not be monotonous.Fig.8 shows the iteration history of T_{cr}.

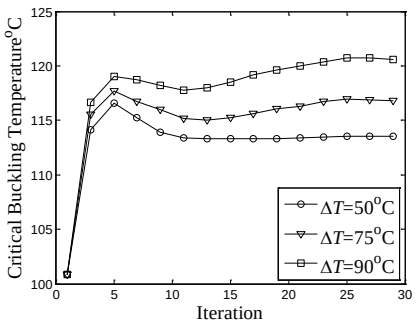

Fig.8 Iteration history of the critical buckling temperature of the case *f*=250Hz

5.2.3. *Case f=1000Hz*

The optimal topology and the iteration history of the SPL are shown in Figs.9 and 10 respectively.

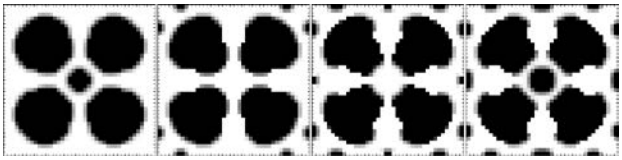

Fig.9 Topology of the bi-material plate (white: material 0; black: material 1) of the case *f*=1000Hz in the four thermal environments a ΔT = 0 °C, b ΔT = 50 °C, c ΔT = 75 °C, d ΔT = 90 °C (from left)

It can be seen that the topology is more complex than that of the cases *f*=50Hz and *f*=250Hz. Generally speaking, the topology remains similar in the four thermal environments.

Fig.11 shows the iteration history of T_{cr}. It can be found that T_{cr} of the subcase ΔT = 50 °C is lower after the optimization; nevertheless, it is still higher than ΔT = 50 °C.

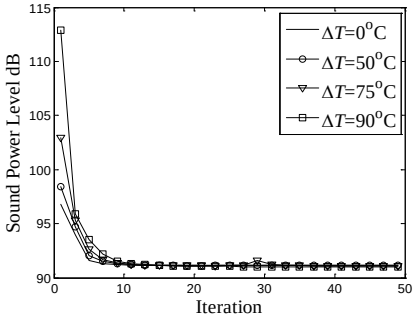

Fig.10 iteration history of the sound power level of the case *f*=1000Hz

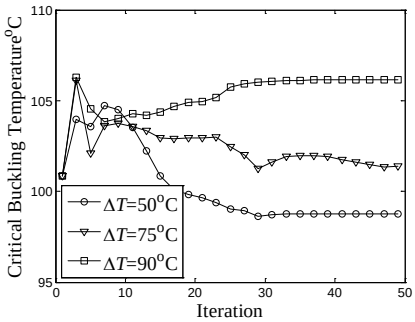

Fig.11 Iteration history of the critical buckling temperature of the case *f*=1000Hz

5.3. *Further discussions*

It can be found that in Yang and Chen et al [2012], the optimal design resembles the contour of the modal shape. This is because that the influence of the design variable, for example ζ_l, on the whole structure was localized at element level, that is, element l. Due to this localization, the sensitivity on ζ_l the only reflects the contribution of the element l to the objective function of the structure. Thus, if the dynamic response at element l is larger, the material of it will be stiffer (i.e. material 1). It also can be concluded that if the load in Yang and Chen et al [2012] were symmetric, the thermal environment would not affect the optimal topology of the structure since the central part would always have lager response than the marginal parts.

In this work, the adjoint method is employed in the sensitivity analysis. The influence of the design variable on the whole structure is completely considered. It can be found that not only the central part but also the margin parts are expected to be stiffer in the optimal design.

The numerical examples in this note are different from those in Yang and Chen et al [2012]. However, this does not reduce the credibility of the comparison, as the numerical examples reflect the characteristics of the sensitivity in both works.

6. Conclusion

In this paper structural topology optimization in a thermal environment with respect to the radiated acoustic characteristic is investigated. The thermal stress is regarded as pre-stress, through which the dynamic formula is obtained to evaluate the structural response. The radiation sound power can then be calculated by Rayleigh integral. Sensitivity analysis is carried out in which how to deal with the derivative of the geometric stiffness matrix is the key point. Both direct and adjoint methods are discussed. In the direct method, the computational cost can be very high for larger-scale problem since a change in one design variable can lead to the variation of the thermal stress of all elements; therefore the geometric stiffness matrices of all elements alter. To carry out the simulation more effectively, the adjoint method is implemented.

A bi-material plate subjected to a harmonic force with prescribed amplitude and frequency is studied. Through buckling and eigenvalue analysis, four pre-buckling thermal cases and three excitation frequency cases are chosen. Numerical results show that as the natural frequencies decrease, SPL varies significantly with the increase of the temperature, especially for the two low-frequency cases. And the optimal topology changes in different thermal environments. It is also shown that the critical buckling temperature basically increases during the optimization process, indicating the structure is always in the pre-buckling state.

Acknowledgment

The assistance on the GCMMA algorithm from Prof. Svanberg K is gratefully acknowledged.

Reference

Akl, W., El-Sabbagh A. and Al-Mitani, K. et al [2009] “Topology optimization of a plate coupled with acoustic cavity,” *Int J Solids Struct* 46, 2060–2074

Bendsøe, M.P. and Sigmund, O. [2003] *Topology optimization theory methods and applications* (Springer. Berlin)

Chen, B., Gu, Y., Zhao, G. et al [2003] “Design optimization for structural thermal buckling,” *J Therm Stresses* 26, 479–494

Christensen, S.T., Sorokin, S.V. and Olhoff, N. [1988] “On analysis and optimization in structural acoustics,” *Struct Optim* 16, 83-107

Cook, R.D. [1994] *Finite Element Modeling for Stress Analysis* (John Willy & Sons. New York)

Du, J. and Olhoff, N. [2007] “Minimization of sound radiation from vibrating bi-material structures using topology optimization,” *Struct Multidisc Optim* 33, 305–321

Du, J. and Olhoff, N. [2010] “Topological design of vibrating structures with respect to optimum sound pressure characteristics in a surrounding acoustic medium,” *Struct Multidisc Optim* 42,43–54

Gao, T. and Zhang, W. [2010] “Topology optimization involving thermo-elastic stress loads,” *Struct Multidisc Optim* 42, 725–738

Kim, N.H. and Dong, J. and Choi, K.K.et,al [2003] “Design sensitivity analysis for a sequential structural–acoustic problem,” *J Sound Vib* 263, 569–591

Lindgaard, E. and Lund, E.[2010] “Nonlinear buckling optimization of composite structures,” *Comput Methods Appl Mech Eng* 199, 2319–2330

Luo, J.H. and Gea, H.G. [2003] “Optimal Stiffener Design for Interior Sound Reduction Using a Topology Optimization Based Approach,” *J Sound Vib* 125, 267-273

Manickarajah, D., Xie, Y.M. and Steven, G.P. [1998] “An evolutionary method for optimization of plate buckling resistance,” *Finite Elements Anal. and Des* 29, 205-230

Pedersen, N.L. [2001] “On topology optimization of plates with prestress,” *Int J Numer Meth Engng* 51, 225–239.

Pedersen, N.L. [2002] “Topology optimization of laminated plates with prestress,” *Computers Structures* 80, 559–570.

Stolpe, M. and Svanberg, K. [2001] “An alternative interpolation scheme for minimum compliance topology optimization,” *Struct Multidisc Optim* 22, 116–124

Svanberg, K. [1987] “The method of moving asymptotes—a new method for structural optimization,” *Int J Numer Methods Engng* 24, 359–373

Svanberg, K. [1995] “A globally convergent version of MMA without linesearch,” *First world congress of structural and multidisciplinary optimization*. Pergamon, Oxford, pp 9–16

Yang, X.W., Chen,G. and Li, Y.M. [2012] “Topology optimization of a bi-material plate with respect to sound radiation in a thermal environment,” *Int J Aerospace and Lightweight Structures* 2, 87-102

Yang, X.W. and Li,Y.M. [2012] “Topology optimization to minimize the dynamic compliance of a bi-material plate in a thermal environment,” *Struct Multidisc Optim*

Yoon, G.H., Jensen, J.S. and Sigmund, O. [2007] “Topology optimization of acoustic-structure interaction problems using a mixed finite element formulation,” *Int J Numer Methods Engng* 70, 1049–1075

Zienkiewicz, O.C. and Taylor, R.L. [2005] *The Finite Element Method for Solid and Structural Mechanics (Sixth edn),* (Butterworth–Heinemann: Elsevier, London.)